Journal of Colloid and Interface Science 374 (2012) 197–205

Contents lists available at SciVerse ScienceDirect

Journal of Colloid and Interface Science

www.elsevier.com/locate/jcis

Crystallization from the micellar phase of imidazolium-based cationic surfactants

Fu-Gen Wu [a], Nan-Nan Wang [a], Qing-Guo Zhang [a,b], Shu-Feng Sun [c], Zhi-Wu Yu [a,*]

[a] Key Laboratory of Bioorganic Phosphorous Chemistry and Chemical Biology, Ministry of Education, Department of Chemistry, Tsinghua University, Beijing 100084, PR China
[b] College of Chemistry and Chemical Engineering, Bohai University, Jinzhou 121000, PR China
[c] Lab of Bio-imaging, The Core Facilities, Institute of Biophysics, Chinese Academy of Sciences, Beijing 100101, PR China

ARTICLE INFO

Article history:
Received 10 November 2011
Accepted 25 January 2012
Available online 4 February 2012

Keywords:
Cationic surfactant
Micelle
Crystallization
Gelation
Submolecular mechanism

ABSTRACT

The self-assembly and phase behavior of the aqueous dispersions consisting of the cationic surfactant, 1-hexadecyl-3-methylimidazolium chloride (C_{16}mimCl), were studied by differential scanning calorimetry, synchrotron small- and wide-angle X-ray scattering, freeze-fracture electron microscopy, polarizing optical microscopy, and Fourier transform infrared spectroscopy. We found that the crystallization of C_{16}mimCl upon cooling is strongly concentration-dependent. At low concentrations (10–25 wt%), the samples change directly from a spherical micellar solution to a lamellar crystalline phase. While at high concentrations (50–67 wt%), the initial cylindrical micelles first convert to the lamellar gel phase and then to the lamellar crystalline phase. Particular efforts have been devoted to unveiling the submolecular mechanisms of the phase transition processes. The transformation from the initial micellar phase to the final crystalline phase upon cooling involves both an ordering rearrangement in the alkyl tails and a dehydrating process in the head region. At high concentrations, the transformation is divided into two steps, *i.e.*, the gelation and subsequent crystallization processes, both involving evident rearrangements of the surfactant tails. Moreover, a significant dehydration of the surfactant head part takes place in the gelation step and a partial rehydration occurs in the crystallization step.

1. Introduction

Imidazolium-based substances have been receiving increasing attention in recent years. One important group is the ionic liquids (ILs) containing 1-alkyl-3-methylimidazolium cations (usually alkyl = ethyl, butyl, and hexyl). Various physiochemical properties of neat imidazolium-based ILs [1–6] and their applications as solvents to assemble amphiphiles have been extensively studied [7–21]. Another important group is the imidazolium-based molecules bearing long alkyl chains (*i.e.*, amphiphilic ILs or AILs). With the possession of long alkyl chains with a carbon number larger than 8, these molecules show typical amphiphilic characteristics and are actually one kind of cationic surfactant. The aggregation behaviors of these surfactants in aqueous solutions have been extensively studied [22–42]. Besides, the amphiphilic nature of the short alkyl chain substituted imidazolium-based molecules has also attracted much attention [31,32,43–45].

The charged surfactants are important building blocks for supramolecular self-assembly targeted to constructing new structures, creating new materials, and obtaining new functions [46–50]. Likewise, the imidazolium-based cationic surfactants which can form various mesophases in water represent a new class of soft matter with potential applications in many fields. Since the structural changes in the self-assembled aggregates consisting of surfactants are usually accompanied by phase state changes, the studies on the phase states and their transformation mechanisms can deepen our understanding on the nature and principle of the self-assembling processes of surfactants. It is thus of interest to have an in-depth understanding of the phase behavior of imidazolium-based cationic surfactants, which are tightly interwoven with the properties and applications of these self-assembled structures. Investigations in this respect, however, are very rare [51,52].

In this work, we have been mainly focusing on the crystallization behavior of the imidazolium-based cationic surfactant upon cooling. It is known that by cooling materials from the melt or fluid phase, metastable phases may occur before converting to stable forms in the later stages [53–57]. The occurrence of the intermediate metastable phases can alter the crystallization pathway, resulting in various structures/morphologies. The physics of the metastable state in aqueous solutions has not been well explored so far due to the lack of metastable states with lifetimes long enough to be investigated [58]. Luckily, our present imidazolium-based cationic surfactant can form long-lived metastable gel phase upon cooling from the fluid micellar phase in aqueous solution. Investigation of such metastable phases can be a key to the understanding of the crystallization process [55].

* Corresponding author. Fax: +86 10 6277 1149.
E-mail address: yuzhw@tsinghua.edu.cn (Z.-W. Yu).

0021-9797/$ - see front matter © 2012 Elsevier Inc. All rights reserved.
doi:10.1016/j.jcis.2012.01.054

For imidazolium-based cationic surfactants, the melt or fluid phases could be micelle solutions, like in the case of common cationic surfactants. The crystallization process of the micelles during cooling should be a fascinating topic, since the metastable phases would concern various self-assembled structures. However, up to date, few efforts have been devoted to understanding the submolecular mechanisms of this process and the relationship between submolecular rearrangement and morphological change. The metastability problem also adds complexity to the phase transition sequences and affects the reversibility and hysteresis of phase transitions. Our present strategy in addressing this problem is to monitor the change of different functional groups of the amphiphilic molecules during phase transitions.

We selected an amphiphilic imidazolium-based ionic liquid, 1-hexadecyl-3-methylimidazolium chloride (C_{16}mimCl, see Fig. 1), to study the self-assembly and phase behavior of C_{16}mimCl aqueous dispersions by using differential scanning calorimetry (DSC), synchrotron small- and wide-angle X-ray scattering (SAXS and WAXS), freeze-fracture electron microscopy (FFEM), polarizing optical microscopy (POM), and Fourier transform infrared (FTIR) spectroscopy. DSC was employed to study the general phase behavior of the C_{16}mimCl–water system. SAXS/WAXS, FFEM, and POM were used to identify the phase states and structures of the samples at selected temperatures. FTIR was applied to reveal the submolecular details of the phase transition processes. In general, we found in the present work that the crystallization behavior of C_{16}mimCl aqueous dispersions is strongly concentration-dependent. At the C_{16}mimCl concentrations of 10 wt%, 17 wt%, and 25 wt%, these samples convert directly from spherical micellar solutions into lamellar crystalline phases upon cooling. While at higher concentrations (50 wt% and 67 wt%), upon cooling, the initial hexagonally packed cylindrical micelles first convert to the lamellar gel phase and then to the lamellar crystalline phase. The formation of the intermediate gel phase en route to the final structure is crucial to the understanding of the crystallization mechanism.

2. Experimental

2.1. Sample preparation

1-Hexadecyl-3-methylimidazolium chloride (C_{16}mimCl) monohydrate (98%) was purchased from Acros Organics. To prepare the C_{16}mimCl aqueous dispersions, double deionized water with a resistivity of 18.2 MΩ cm or D_2O (99.9% of deuterium, from Cambridge Isotopes) was used. The concentrations of C_{16}mimCl were 10 wt%, 17 wt%, 25 wt%, 33 wt%, 50 wt%, and 67 wt%. Homogeneous dispersions were prepared by repeated thermal cycles between −20 and 50 °C. The samples with lower C_{16}mimCl concentrations (10–25 wt%) are clear solutions at room temperature. For the samples with higher C_{16}mimCl concentrations (33–67 wt%), vigorous stirring at 50 °C was applied for 5 min. The homogeneity of these suspensions was checked by the appearance of identical DSC thermograms for the samples taken from different positions of the suspension.

2.2. DSC

Calorimetric data were obtained with a differential scanning calorimeter DSC821^e equipped with the high-sensitivity sensor HSS7 (Mettler-Toledo Co., Switzerland). The scan rate was 0.5 °C/min.

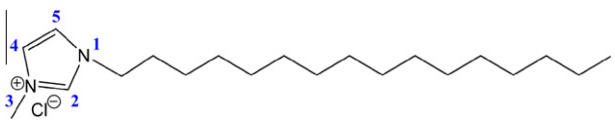

Fig. 1. Molecular structure of C_{16}mimCl.

2.3. Synchrotron X-ray diffraction

SAXS and WAXS experiments were at the beam line 1W2A of the Beijing Synchrotron Radiation Facility (BSRF) (λ = 1.54 Å). A standard silver behenate sample was used for the calibration of diffraction spacings. X-ray scattering intensity patterns were recorded during 60 s exposure of the samples to the synchrotron beam. To obtain the SAXS and WAXS data simultaneously, we fixed the sample to detector distance at 450 mm. A Linkam thermal stage (Linkam Scientific Instruments, the United Kingdom) was used for temperature control (±0.1 °C). The X-ray powder diffraction intensity data were analyzed using the program Fit2D.

2.4. FFEM

Freeze-fracture electron microscopy (FFEM) technique was used to characterize the morphology of the two C_{16}mimCl aqueous dispersions (25 wt% and 50 wt%) at 30 °C. Samples and tools used for sample manipulation were equilibrated at the desired temperature for at least 5 min. A suitable amount of the suspension was mounted onto the sample holder and manually plunged into the liquid ethane cooled by the liquid nitrogen in advance. After that the samples were stored in the liquid nitrogen. The freeze-fracture procedure was carried out in a Balzers BAF 400D freeze-fracture apparatus at −120 °C, 3×10^{-7} mbar. Fractured surfaces were shadowed with platinum/carbon. Platinum and carbon evaporation was done from 45° and 90° angle, with the thickness of 20 Å and 150 Å, respectively. Replicas were cleaned by floating onto water or water–methanol solvent. Images were then recorded with a JEOL 2010 transmission electron microscope (JEOL Ltd., Tokyo, Japan).

2.5. POM

A polarizing optical microscope (Olympus BX51) was used to observe the phases formed by the samples with C_{16}mimCl concentrations of 25 wt% and 50 wt% at 30 °C. A small amount of the sample was sandwiched between two thin glass plates. The temperature (30 °C) was controlled using a Linkam LTS350 hot stage.

2.6. FTIR spectroscopy

FTIR spectra were recorded using a Nicolet 5700 Fourier transform infrared spectrometer with a DTGS detector in the range of 4000–900 cm^{-1} with a spectral resolution of 2 cm^{-1} and a zero filling factor of 2. Samples were coated onto the inner surfaces of a pair of CaF_2 windows separated by a 6 μm (for C_{16}mimCl–H_2O) or 25 μm (for C_{16}mimCl–D_2O) Teflon spacer. A piece of Parafilm was used to wrap the surroundings of the two CaF_2 windows, which were then mounted on a Linkam heating–cooling stage for temperature control (±0.1 °C). 32 scans were carried out for each spectrum.

3. Results and discussion

3.1. DSC

Fig. 2 shows the DSC results of the C_{16}mimCl–H_2O systems upon cooling and subsequent heating scans at 0.5 °C/min. In the cooling scans (Fig. 2a), for the samples with the C_{16}mimCl concentrations of 10 wt%, 17 wt%, and 25 wt%, only one exothermic peak centered

at ~4 °C was observed. As demonstrated below, this is the fluid phase to crystalline phase transition process. At 33 wt%, a complex transition pattern was observed and the exothermic peak starts at ~13 °C and lasts until 3 °C. At 50 wt%, two transition regions over 18–11 °C and 5–2 °C are seen. At 67 wt%, there are also two transition regions over 23–11 °C and 6–2 °C. The two transition regions may correspond to a two-step thermal event. As demonstrated below, this two-step event corresponds to a fluid to gel and gel to crystalline phase transitions. For the 50 wt% and 67 wt% samples, their first- and second-step transition upon cooling have almost identical enthalpy change, *i.e.*, −28.8 ± 2.3 kJ/mol and −26.4 ± 1.5 kJ/mol, respectively. A comparison of the onset temperatures of the first-step transition process also indicates that it is easier to take place at higher C_{16}mimCl concentrations (or at lower water contents). Interestingly, for each of these six samples, the total enthalpy change of the exothermic transitions upon cooling is almost the same, −53.4 ± 2.6 kJ/mol. Upon subsequent heating (Fig. 2b), we can see that at higher C_{16}mimCl concentrations, the endothermic transitions become more complex, and the phase transition processes finish at higher temperatures: 14.8 °C at 10 wt%, 15.9 °C at 17 wt%, 16.6 °C at 25 wt%, 17.4 °C at 33 wt%, 20.5 °C at 50 wt%, and 25.2 °C at 67 wt%. The total enthalpy change of the endothermic transitions for each of these six samples upon heating is almost the same, *i.e.*, 55.4 ± 1.7 kJ/mol. Thus, if we only consider the phase states at the starting and ending point (not the transition pathways), we can say that for each of these six samples, they undergo reversible phase transitions upon cooling and subsequent heating processes with almost the same enthalpy change values. For the 10 wt%, 17 wt%, and 25 wt% samples, the differences in the phase transition temperatures of the crystalline ↔ fluid phase transformations upon heating and cooling indicate a significant hysteresis effect (According to the onset temperatures of the heating and cooling scans, the temperature difference is about 5 °C.). This is due to the difficulty in the nuclei formation of the crystalline phase upon cooling from the fluid phase.

According to the above DSC cooling results, the 25 wt% and 50 wt% samples represent two typical phase transition types, and we will study in detail the phase behavior of these two samples upon cooling. Besides, since the DSC cooling results of C_{16}mimCl–D_2O systems for the 25 wt% and 50 wt% samples gave almost identical phase behaviors as those of the C_{16}mimCl–H_2O systems at the same concentrations (data not shown), the results allow us to study the phase transition processes of C_{16}mimCl–H_2O by using C_{16}mimCl–D_2O in our FTIR experiments.

To more clearly present the phase behavior of C_{16}mimCl–H_2O system, a *T*–*X* partial phase diagram was constructed by plotting the phase transition onset temperature as a function of the composition. Here we did not use the peak transition temperatures since they depend strongly on the DSC heating rates. Note that to draw this phase diagram, additional DSC measurements were carried out for samples with the C_{16}mimCl concentrations of 29 wt%, 39 wt%, 45 wt%, 56 wt%, and 62 wt% (data not shown). The thus obtained phase diagram in Fig. 3 is similar to that of the C_{12}mimBr–H_2O system [52]. From Fig. 3, we can see that at low temperatures, the solid or crystalline phase (S) forms, while at high temperatures, the fluid phase in the spherical micellar (M) or hexagonal phase (H_1) forms. The following X-ray, FFEM, and POM have been used to confirm the formation of these different phases. We should also mention that since the gel phase is the metastable phase formed only upon cooling and is thus not included in the phase diagram.

3.2. SAXS and WAXS

Shown in Fig. 4 are the X-ray scattering results of two selected C_{16}mimCl–H_2O samples. For the sample with the C_{16}mimCl concentration of 25 wt% (Fig. 4a), we can see that the small-angle region (the left part of the curve) at 30 °C shows only one peak centered at q_m = ~1.0 nm^{-1}. This is an intermicelle interference peak, which indicates the correlation length (ξ_C) of pair distribution function of micelles [58]. The peak usually occurs at $q_m = 2\pi/\xi_C$, and the thus obtained ξ_C is ~6.3 nm. The q_m value of ~1.0 nm^{-1} in our 25 wt% C_{16}mimCl sample is comparable with that (0.9–1.0 nm^{-1}) of the concentrated cetyltrimethylammonium chloride (CTAC) micellar solution (700 mM, or 224 g/L) [59], which can support our above analysis. The wide-angle region shows a very diffuse peak at q_m = ~14 nm^{-1}, corresponding to a repeat distance $d = 2\pi/q_m$ = 0.45 nm. The *d* value reflects the packing tightness of the hydrocarbon chains of the surfactant tails and the value of 0.45 nm indicates that the sample at 30 °C is in a fluid state [60,61].

When cooling to 0 °C, we can see from the left part of the curve (the SAXS data) that the scattering vector maxima (q_m) show a ratio of 1:2:3:4:5, indicating that the sample is lamellar-structured. From the *q* values, we can obtain the repeat distances using the equation $d = 2\pi/q$. The thus obtained average *d* value is 3.2 nm. Be-

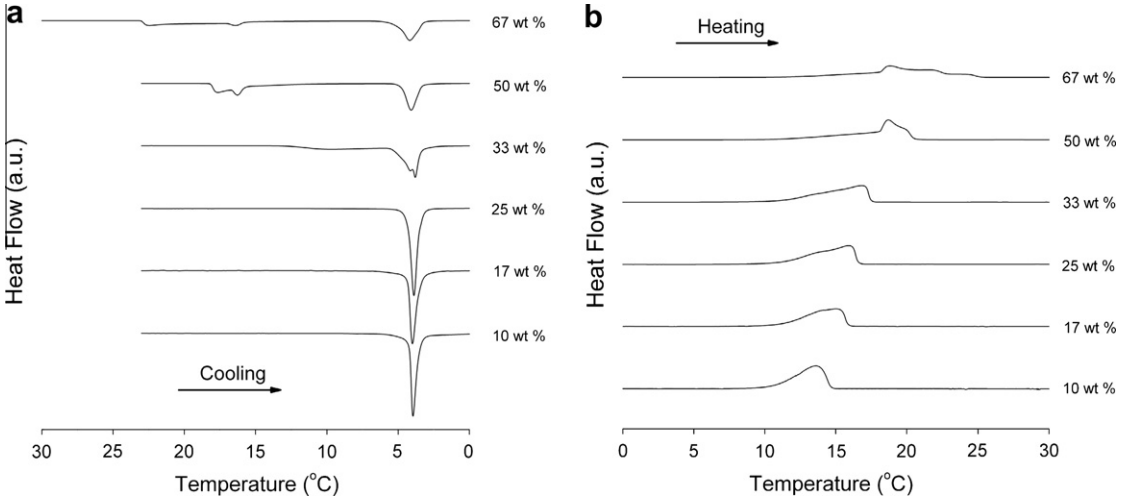

Fig. 2. DSC results of the C_{16}mimCl–H_2O systems upon cooling: (a) and subsequent heating and (b) scans at 0.5 °C/min. Weight percentages of the surfactants in the mixtures are tagged to the respective curves.

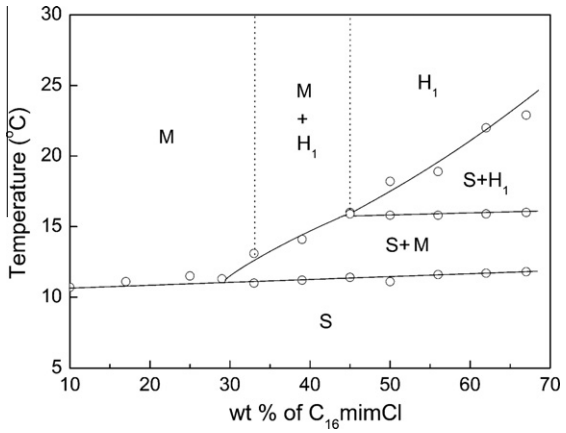

Fig. 3. Phase diagram of C_{16}mimCl–H_2O system. S (solid phase of C_{16}mimCl), H_1 (hexagonal phase), M (spherical micellar phase).

sides these periodical peaks, some other peaks mainly residing in the region of $q > 12\ nm^{-1}$ come from the tight, ordered packing of the alkyl chains, suggesting that the sample is in crystalline phase. As the bilayer thickness (3.2 nm) is smaller than the sum of two fully stretched C_{16}mimCl molecules (~5 nm, derived by MM2 force field simulation in the absence of the counterion Cl^-), we may expect that the alkyl chains in this lamellar crystalline phase are interdigitated and/or tilted.

For the sample with the C_{16}mimCl concentration of 50 wt% (Fig. 4b), at 30 °C, the broad peak in the WAXS region proves that the sample is in a fluid phase. The SAXS peaks show a q_1 (100):q_2 (110):q_3 (200):q_4 (210) = 1:√3:(2):√7 pattern (the intensity of the q_3 peak is very low), suggesting the formation of the hexagonally packed cylindrical micellar phase (the H_1 phase). From the 100 plane of the hexagonal lattice (together with other reflections such as 110 and 210) we can calculate the interlayer spacing d of the H_1 phase [62], and the thus obtained value is 4.5 nm. When the sample was cooled to 7 °C, several periodical Bragg peaks show a ratio of q_1:q_2:q_3:q_4:q_5:q_6 = 1:2:3:4:(5):6 (the intensity of the fifth order is too low to be seen), suggesting the formation of a multilamellar structure. The calculated repeat distance (d) is 5.1 nm. In the WAXS region, the peak at $q_m = 15.4\ nm^{-1}$ (or d = 0.41 nm) indicates that the sample was in a gel state. Moreover, as the WAXS data can reflect the carbon–carbon packing information in the alkyl chains, the smaller d value (0.41 nm) indicates that the packing is tighter than the conventional lamellar gel phase which has a d value of 0.42–0.43 nm [60,63,64]. The result may suggest the formation of an interdigitated (or partially interdigitated) structure, in which the alkyl chains of the C_{16}mimCl molecules from the opposing monolayers are interpenetrated. Upon further cooling to 0 °C, the X-ray scattering profile at 0 °C is almost the same as that for the 25 wt% sample at 0 °C, which means that the same multilamellar crystalline phase was formed.

3.3. FFEM

To further confirm the phase states of the 25 wt% and 50 wt% samples at 30 °C, we also carried out FFEM measurements for the two samples, and the results are shown in Fig. 5. Photographs of the samples in glass vials are also included in the figure to show their physical appearances at 30 °C. For the 25 wt% sample (Fig. 5a), the transparent feature as shown in the photograph of the sample in the glass vial is characteristic of an isotropic solution. FFEM reveals that spherical aggregates with sizes ranging from 10 to 20 nm predominate in the sample solution. Investigations of the 10 wt% and 17 wt% samples show almost the same results as those of the 25 wt% sample, indicating that the 10–25 wt% samples are spherical micellar solutions at 30 °C. For the 50 wt% sample, the photograph (the inset in Fig. 5b) shows that the sample is hydrated and fluid-like (lyotropic liquid crystal). FFEM results (Fig. 5b and c) reveal that cylindrical aggregates with a diameter of ~7 nm and lengths of >500 nm are seen in the dispersion. The combination of FFEM and X-ray scattering results suggests the formation of H_1 phase at 30 °C for the 50 wt% sample. Note that the FFEM data cannot reflect the hexagonal packing geometry, possibly due to the freeze-fracture sample preparation procedure. The formation of H_1 phase in C_{16}mimCl can be supported by the results obtained from other similar-structured imidazolium-based surfactants such as 1-dodecyl-3-methylimidazolium bromide (C_{12}mimBr) [52] and *N*-hexadecyl-*N*-methylpyrrolidinium bromide (C_{16}MPB) [65], which also form H_1 phase in water at high concentrations.

3.4. POM

Another very classical method to investigate the isotropic or anisotropic nature of the self-assembled aggregates is polarizing optical microscopy (POM). For the 25 wt% sample, the POM image taken at 30 °C only shows the background (Fig. 6a), which is the characteristic of a homogeneous and isotropic phase (isotropic

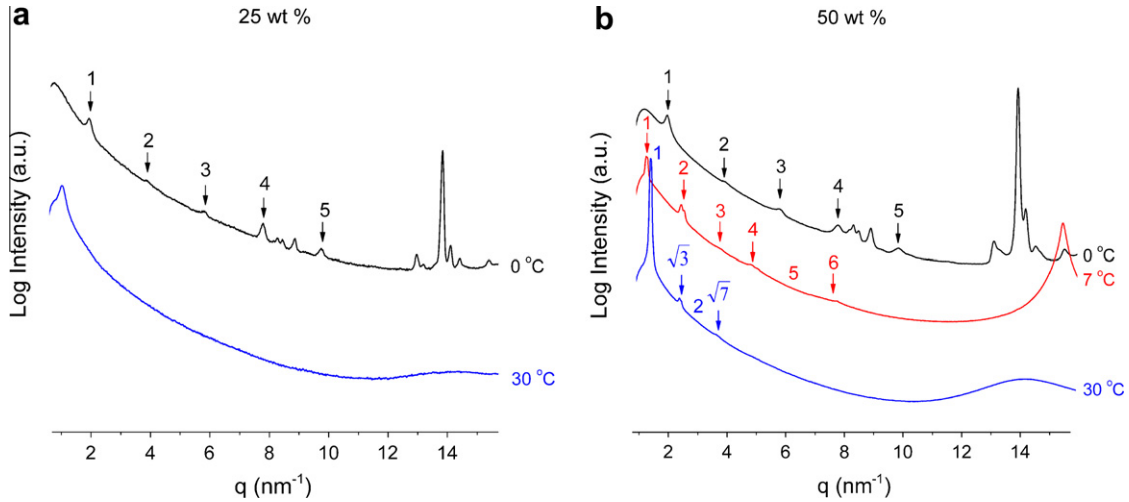

Fig. 4. Synchrotron X-ray scattering results of C_{16}mimCl–H_2O. (a) 25.0 wt% at 30 °C and 0 °C, (b) 50.0 wt% at 30 °C, 7 °C, and 0 °C.

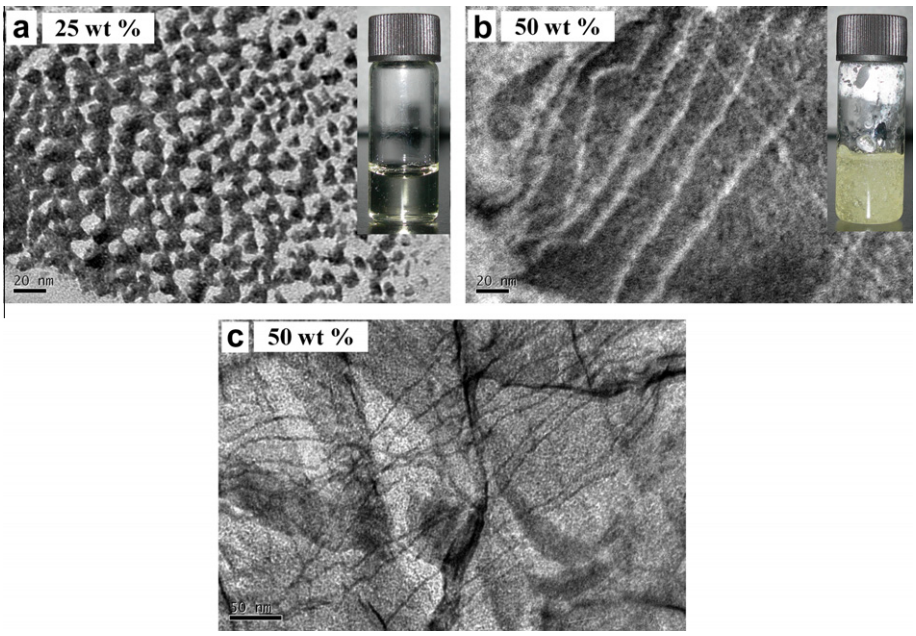

Fig. 5. (a) FFEM image of the 25 wt% C_{16}mimCl–H_2O sample at 30 °C. (b and c): FFEM images of the 50 wt% C_{16}mimCl–H_2O sample at 30 °C. The insets in (a and b) are the photographs of the two samples at 30 °C in glass vials.

spherical micelles). While for the 50 wt% sample at 30 °C, clear birefringent regions can be seen in the POM image (Fig. 6b), indicating the anisotropic nature of the sample. The textures observed in this sample are very similar to those in other POM images of the H_1 phase [52,62,66–68]. Hence, with the POM images and the above X-ray and FFEM results, we can confirm the formation of the fluid spherical micelles in the 25 wt% sample and the fluid hexagonal phase in the 50 wt% sample at 30 °C.

3.5. FTIR

To provide a submolecular understanding on the phase behavior of C_{16}mimCl aqueous dispersions, we have carried out FTIR experiments with the two samples containing 25 wt% and 50 wt% C_{16}mimCl.

The FTIR absorbance spectra for the C_{16}mimCl–H_2O systems at some selected temperatures during cooling from 30 to 0 °C at 0.5 °C/min are shown in Fig. 7. Fig. 7a is the result of the fluid spherical micellar phase (30 °C) and the lamellar crystalline phase (0 °C) of the 25 wt% sample. The 2880–2820 cm^{-1} region contains the CH_2 symmetric stretching band ($\nu_s CH_2$) of the long alkyl chains in the surfactant tail region [69]. The spherical fluid micellar phase to the multilamellar crystalline phase transition is characterized by a band shift toward low wavenumber and a sharpening of the band width. At the spherical fluid micellar phase (30 °C), the $\nu_s CH_2$ band locates at 2853.4 cm^{-1}. It shifts to 2849.5 cm^{-1} in the multilamellar crystalline phase at 0 °C. These special features have been used frequently to follow the conformational order of the alkyl chains and the *gauche–trans* isomerization of the CH_2 groups in the surfactant tail regions [57,69–73]. The result shows that during the micellar to crystalline transition, the *trans* conformers in the long alkyl chains increase significantly. Another important band is the CH_2 scissoring vibration (δCH_2) in the long alkyl chains, which is very sensitive to the intermolecular forces, and can be served as a key band for examining the state of packing of the methylene chains in various phases [57,69–73]. At 30 °C in the spherical micellar phase, the very broad band at 1467.4 cm^{-1} suggests that the long alkyl chains are in the disordered or fused state. At 0 °C

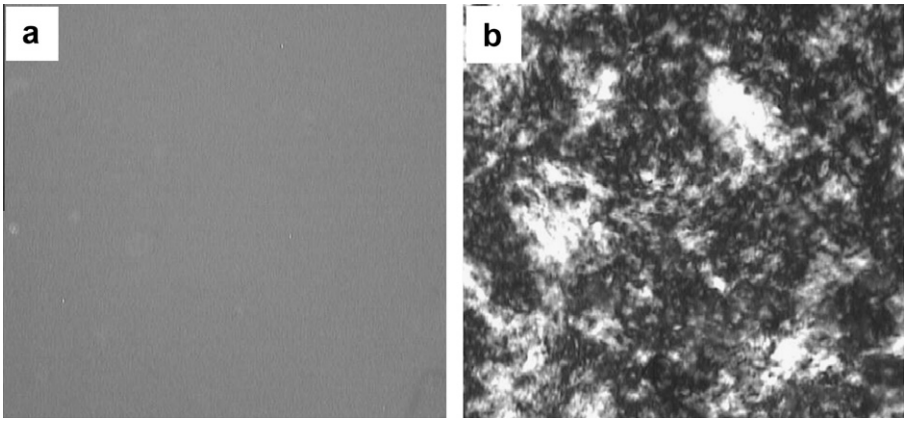

Fig. 6. POM images of C_{16}mimCl–H_2O mixtures at 30 °C. (a) 25 wt%, (b) 50 wt%.

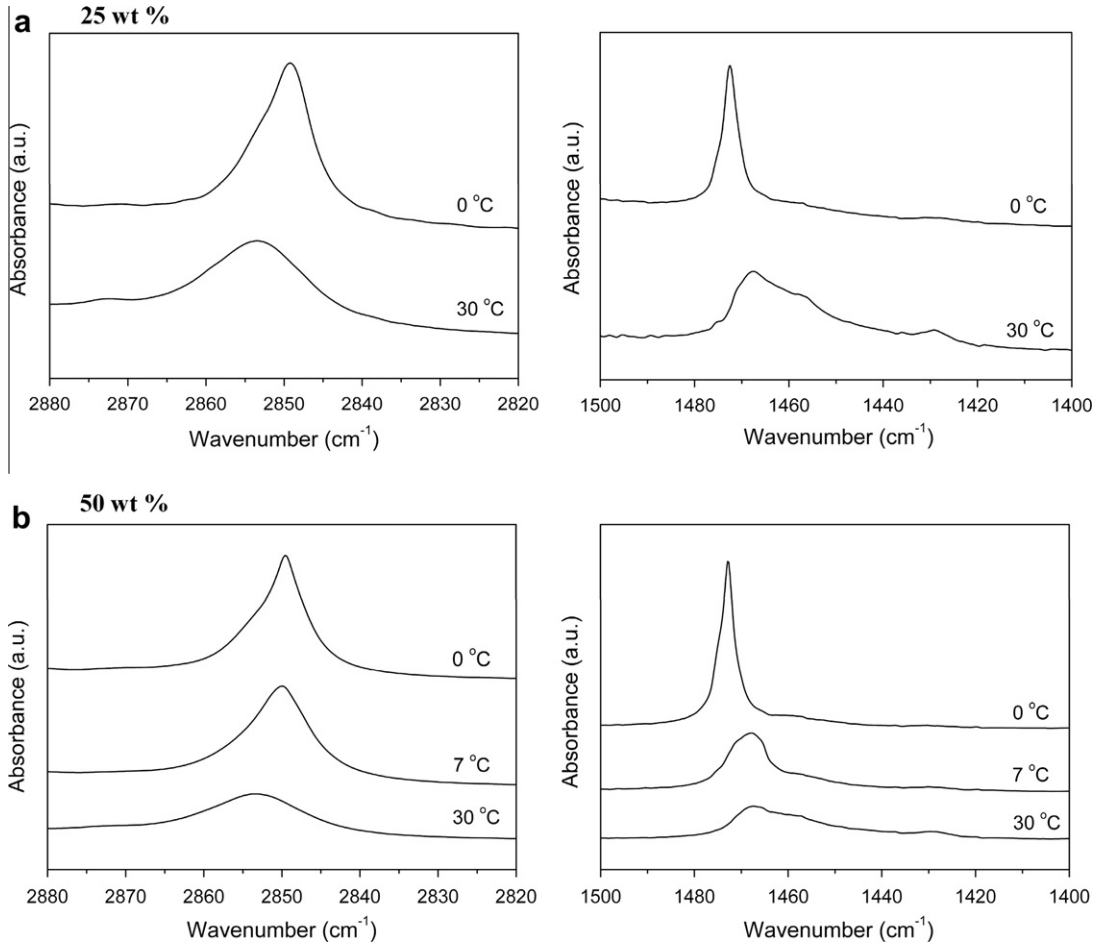

Fig. 7. FTIR spectra (2880–2820 and 1500–1400 cm^{-1} regions) of C_{16}mimCl–H_2O at selected temperatures during cooling from 30 to 0 °C at 0.5 °C/min. (a) 25.0 wt%, (b) 50.0 wt%.

in the crystalline phase, on the other hand, the presence of a single and relatively sharp peak at 1472.9 cm^{-1} indicates that the methylene *trans*-zigzag planes are packed in an ordered triclinic state.

In Fig. 7b, for the 50 wt% sample, we can see that the spectrum for the cylindrical micellar phase at 30 °C is almost the same as that for the spherical micellar phase at 30 °C in Fig. 7a. This indicates that the two types of micelles have almost the same conformation and packing. When cooling to 7 °C, the intermediate gel phase forms. The shift of the $\nu_s CH_2$ band from 2853.3 cm^{-1} at 30 °C to 2850.0 cm^{-1} at 7 °C indicates a significant increase of the *trans* conformers in the long alkyl chains. For δCH_2 at 1467.9 cm^{-1}, its band shape is similar to that of the cylindrical micellar state at 30 °C. But by careful comparison, we can see that it is a little sharper. Based on the literature [69], the characteristics of the band shape and band position suggest that the alkyl chains are in a hexagonal packing state. But on the whole, the long alkyl chains are loosely packed in both the cylindrical micellar and lamellar gel phases as their δCH_2 bands are still very broad.

Upon further cooling to 0 °C, the crystalline phase forms. In this phase, we found that the $\nu_s CH_2$ band residing at 2849.6 cm^{-1} is very similar to that in the gel phase at 7 °C. The similar band shape and band position of the samples at 7 °C and 0 °C indicates that the *trans* conformers predominate in both the gel and the crystalline phases, and the conformational changes in the alkyl chains during the gel to crystalline phase transition are small. However, a marked change of δCH_2 was observed. It shifts from 1467.9 to 1472.9 cm^{-1}, accompanied by a significant narrowing of the band width. The results indicate that this is a conversion of a loose, hexagonal packing to a tight, triclinic packing, and the intermediate gel phase transforms into the final crystalline phase.

To study the hydrogen bonding interaction changes involving the imidazolium cations of the C_{16}mimCl molecules, the CH stretching vibrations in the positions 2, 4, and 5 of the imidazolium ring ($\nu C_{(2)}$–H and $\nu C_{(4,5)}$–H) at 3200–3050 cm^{-1} are frequently used as the spectral probes to study the cation–anion and cation–solvent interactions [74–86]. However, these bands are very weak in band intensities and are severely affected by the strong H_2O absorption in the 3700–3000 cm^{-1} region in our C_{16}mimCl–H_2O samples (data not shown). Thus, the C_{16}mimCl–D_2O samples were used instead to improve the spectral quality. As the DSC cooling results for the C_{16}mimCl–D_2O samples (25 wt% and 50 wt%) are almost the same as those for the C_{16}mimCl–H_2O samples at the same concentrations, it is reasonable to interpret the IR results based on the C_{16}mimCl–D_2O systems. In Fig. 8, the 3200–3050 cm^{-1} region contains roughly two absorption regions, the one at 3190–3125 cm^{-1} is assigned to $\nu C_{(4,5)}$–H, and the other at 3125–3060 cm^{-1} is assigned to $\nu C_{(2)}$–H [83,85]. For the 25 wt% sample (Fig. 8a), the difference between the $\nu C_{(4,5)}$–H bands at 30 °C and 0 °C reflects that the change in the conformation or environment of $C_{(4,5)}$–H during the micellar to crystalline phase transition. Similarly, for the 50 wt% sample (Fig. 8b), the differences between the $\nu C_{(4,5)}$–H bands at 30 °C, 7 °C, and 0 °C reflect the changes in the conformation or environment of $C_{(4,5)}$–H during the micellar to gel and gel to crystalline phase transitions.

As it has been reported that the most favorable site for an imidazolium cation to H-bond to an anion or a solvent molecule is the

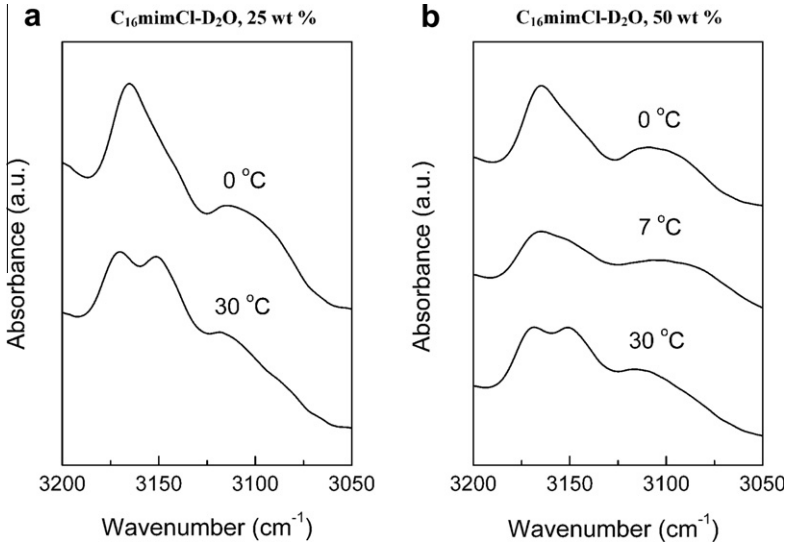

Fig. 8. FTIR spectra (3200–3050 cm^{-1} region) of C_{16}mimCl–D_2O at selected temperatures during cooling from 30 to 0 °C at 0.5 °C/min. (a) 25.0 wt%, (b) 50.0 wt%.

$C_{(2)}$–H [74–83,84–86], the $\nu C_{(2)}$–H band is sensitive to the change of hydrogen bonding strength of the imidazolium cation. For the 25 wt% sample, the downward shift (~5 cm^{-1}) of the band position during the micellar (30 °C) to crystalline (0 °C) suggests an increase in the hydrogen bonding strength between the $C_{(2)}$–H in the ring and the hydrogen bond acceptors. According to the previous surveys [75,76,78], the hydrogen bonding interaction between imidazolium cation and counterion (which is a charge-enhanced hydrogen bonding interaction) is stronger than that between imidazolium cation and water. Thus, the increase in the hydrogen bonding strength indicates a partial dehydration of the imidazolium cation. For the 50 wt% sample, the downward shift (from ~3114 to ~3104 cm^{-1}) in the band position during the micellar (30 °C) to gel (7 °C) transition suggests the dehydration of the imidazolium cation, while the upward shift (from ~3104 to ~3109 cm^{-1}) in the band position during the gel (7 °C) to crystalline (0 °C) transition suggests a partial rehydration of the imidazolium cation. However, from the initial micellar phase to the final crystalline phase, the imidazolium cation dehydrates.

3.6. Concentration-dependent crystallization of the C_{16}mimCl aqueous dispersions

In this work, we observed reversible spherical micelle–lamellar crystalline phase transformations upon cooling and heating for the samples with lower C_{16}mimCl concentrations (10 wt%, 17 wt%, and 25 wt%). This is a typical Krafft transition for surfactants. For the samples with higher C_{16}mimCl concentrations (50 wt% and 67 wt%), hexagonally packed cylindrical micelles form at high temperatures. Upon cooling, these cylindrical micelles first convert to the intermediate lamellar gel phase and then transform into the final lamellar crystalline phase.

For the two types of micelles (spherical micelle in 25 wt% sample and cylindrical micelle in 50 wt% sample), we found that no significant difference in the conformation, packing, and hydration as revealed by FTIR at 30 °C. Accordingly, when these two micelles undergo phase transitions from the initial micellar phase to the final crystalline phase upon cooling, almost identical enthalpy changes are obtained, with the fact in mind that the final crystalline phases for the two samples are exactly the same, as revealed by SAXS/WAXS and FTIR.

The formation of different phases with various morphologies can be explained by the critical packing parameter P_c, using the equation $P_c = V/(al)$, where V is the surfactant tail volume, a is the effective headgroup area, and l is the extended length of the alkyl chain, respectively [87,88]. When $P_c < 1/3$, spherical micelles form. At $1/3 < P_c < 1/2$, cylindrical or rod-shaped micelles form. When P_c approaches 1, lamellar structures form. The relative sizes of the head and tail parts of the C_{16}mimCl molecules are affected by the hydration and mobility of the head part and the conformation and packing of the alkyl chain tails. For the 25 wt% sample, the sufficient water content ensures a large, well-hydrated headgroup with a high mobility. This may lead to a P_c value <1/3, and thus spherical micelles form. For the 50 wt% sample, the fewer amounts of water molecules available in the suspension lead to a higher concentration of the counterions (Cl^-) around the imidazolium cations, and thus increasing the bindings between the imidazolium cations and the counterions (Cl^-). This results in a restricted mobility of the micellar polar heads and a decreased effective headgroup area, leading to $1/3 < P_c < 1/2$. Then, cylindrical micelles form. Upon cooling the 50 wt% sample to 7 °C, from the band width changes of δCH_2 as shown in Fig. 7b, we can see that the cylindrical micellar state at 30 °C and the gel state at 7 °C are both loosely packed, with the latter a little tighter than the former, and thus the changes of V and l (or V/l) may be insignificant. Meanwhile, the significant dehydration of the head part largely decreases a_0, which makes P_c approach 1, leading to the formation of the lamellar gel phase. When the sample was cooled to 0 °C, the rigidifying of the alkyl chains and the partial rehydration of the polar headgroups can still guarantee a P_c value of ~1, leading to the formation of the lamellar crystalline phase. The case is similar for the 25 wt% sample when cooling to 0 °C.

4. Conclusions

We have studied the self-assembly and phase behavior of C_{16}mimCl aqueous dispersions by using DSC, SAXS/WAXS, FFEM, POM, and FTIR techniques. We found that the phase behavior of the system depends largely on the water content of the sample. At 30 °C, spherical micellar solutions form in the 10–25 wt% C_{16}mimCl samples, while cylindrical micellar phases (lyotropic liquid crystals) form in the 50–67 wt% C_{16}mimCl samples. Upon cooling, the spherical micellar solution directly converts to the

lamellar crystalline phase, while the cylindrical micellar phase first converts to the lamellar gel phase and then to the lamellar crystalline phase.

Despite some previous studies [51,52] on the phase behavior of imidazolium-based surfactants in aqueous solutions, a detailed investigation on the submolecular mechanisms of the phase transitions of the imidazolium-based surfactants is still lacking. By using FTIR, we found that the transformation from the initial spherical or cylindrical micellar phase to the final crystalline phase upon cooling involves both an ordering rearrangement in the alkyl tails and a dehydrating process in the head region. For the 50 wt% sample, upon cooling from the initial cylindrical micellar phase, the two steps, *i.e.*, the gelation and subsequent crystallization processes, both involve evident rearrangements of the surfactant tails. Moreover, marked dehydration of the surfactant head part takes place in the first gelation step and a partial rehydration occurs in the second crystallization step.

Knowledge of the submolecular characterization on the phase transformation process sets the foundation for the modulation of the formation kinetics or even the formation pathway of the desired crystalline materials. On one hand, understanding the crystallization pathway enables us to optimize the experimental conditions to produce single crystals of surfactants large enough for further X-ray structural analysis. On the other hand, since many surfactant molecules are insolubilized and solidified with decreasing temperatures of the aqueous surfactant solutions [89,90], the present work may have implications for the purification of surfactants. It also opens the door for us to seek the specific conditions to prevent the micellar phase from gelation or crystallization if the fluid micellar phase is needed in some specific applications. Besides, our work shows that the relatively long-lived metastable gel phase can be regarded as the preordering stage toward the final crystalline phase. The formation of a preordered structure prior to the final crystalline state can deepen our understanding on the crystallization mechanisms of surfactants and should thus be widely recognized and explored.

Acknowledgments

This work was supported by grants from the Natural Science Foundation of China (Grant No. 20973100 and 21133009). The SAXS and WAXS data were collected at the beam line 1W2A of the Beijing Synchrotron Radiation Facility (BSRF) with the assistance of Dr. Zhong-Hua Wu and Guang Mo. We also appreciate the help from Yin Jiang (Department of Chemistry, Tsinghua University) on the POM experiment.

References

[1] M. Tariq, A.P. Serro, J.L. Mata, B. Saramago, J.M.S.S. Esperanca, J.N. Canongia Lopes, L.P.N. Rebelo, Fluid Phase Equilib. 294 (2010) 131.
[2] M. Blesic, M. Swadźba-Kwaśny, T. Belhocine, H.Q.N. Gunaratne, J.N. Canongia Lopes, M.F.C. Gomes, A.A.H. Padua, K.R. Seddon, L.P.N. Rebelo, Phys. Chem. Chem. Phys. 11 (2009) 8939.
[3] A.E. Bradley, C. Hardacre, J.D. Holbrey, S. Johnston, S.E.J. McMath, M. Nieuwenhuyzen, Chem. Mater. 14 (2002) 629.
[4] J.D. Holbrey, K.R. Seddon, J. Chem. Soc., Dalton Trans. 13 (1999) 2133.
[5] A. Stoppa, O. Zech, W. Kunz, R. Buchner, J. Chem. Eng. Data 55 (2010) 1768.
[6] O. Zech, A. Stoppa, R. Buchner, W. Kunz, J. Chem. Eng. Data 55 (2010) 1774.
[7] R.H. Dong, J.C. Hao, Chem. Rev. 110 (2010) 4978.
[8] T.L. Greaves, C.J. Drummond, Chem. Soc. Rev. 37 (2008) 1709.
[9] B.P. Binks, A.K.F. Dyab, P.D.I. Fletcher, Phys. Chem. Chem. Phys. 9 (2007) 6391.
[10] Y.A. Gao, N. Li, L.Q. Zheng, X.Y. Zhao, S.H. Zhang, B.X. Han, W.G. Hou, G.Z. Li, Green Chem. 8 (2006) 43.
[11] Y.A. Gao, S.B. Han, B.X. Han, G.Z. Li, D. Shen, Z.H. Li, J.M. Du, W.G. Hou, G.Y. Zhang, Langmuir 21 (2005) 5681.
[12] J. Eastoe, S. Gold, S.E. Rogers, A. Paul, T. Welton, R.K. Heenan, I. Grillo, J. Am. Chem. Soc. 127 (2005) 7302.
[13] K.A. Fletcher, S. Pandey, Langmuir 20 (2004) 33.
[14] H.X. Gao, J.C. Li, B.X. Han, W.N. Chen, J.L. Zhang, R. Zhang, D.D. Yan, Phys. Chem. Chem. Phys. 6 (2004) 2914.
[15] B.P. Binks, A.K.F. Dyab, P.D.I. Fletcher, Chem. Commun. (2003) 2540.
[16] J.L. Anderson, V. Pino, E.C. Hagberg, V.V. Sheares, D.W. Armstrong, Chem. Commun. (2003) 2444.
[17] T.L. Merrigan, E.D. Bates, S.C. Dorman, J.H. Davis Jr., Chem. Commun. (2000) 2051.
[18] O. Zech, S. Thomaier, P. Bauduin, T. Rück, D. Touraud, W. Kunz, J. Phys. Chem. B 113 (2009) 465.
[19] A. Harrar, O. Zech, A. Klaus, P. Bauduin, W. Kunz, J. Colloid Interface Sci. 362 (2011) 423.
[20] A. Harrar, O. Zech, R. Hartl, P. Bauduin, T. Zemb, W. Kunz, Langmuir 27 (2011) 1635.
[21] O. Zech, W. Kunz, Soft Matter 7 (2011) 5507.
[22] H.Y. Wang, Q.Q. Feng, J.J. Wang, H.C. Zhang, J. Phys. Chem. B 114 (2010) 1380.
[23] M. Blesic, M. Swadźba-Kwaśny, J.D. Holbrey, J.N. Canongia Lopes, K.R. Seddon, L.P.N. Rebelo, Phys. Chem. Chem. Phys. 11 (2009) 4260.
[24] B. Chamiot, C. Rizzi, L. Gaillon, J. Sirieix-Plénet, J. Lelièvre, Langmuir 25 (2009) 1311.
[25] Y.Y. Lin, Y. Qiao, Y. Yan, J.B. Huang, Soft Matter 5 (2009) 3047.
[26] H.Y. Wang, J.J. Wang, S.B. Zhang, X.P. Xuan, J. Phys. Chem. B 112 (2008) 16682.
[27] Y. Zhao, S.J. Gao, J.J. Wang, J.M. Tang, J. Phys. Chem. B 112 (2008) 2031.
[28] J. Łuczak, J. Hupka, J. Thöming, C. Jungnickel, Colloids Surf., A 329 (2008) 125.
[29] B. Dong, X.Y. Zhao, L.Q. Zheng, J. Zhang, N. Li, T. Inoue, Colloids Surf., A 317 (2008) 666.
[30] B. Dong, J. Zhang, L.Q. Zheng, S.Q. Wang, X.W. Li, T. Inoue, J. Colloid Interface Sci. 319 (2008) 338.
[31] I. Goodchild, L. Collier, S.L. Millar, I. Prokeš, J.C.D. Lord, C.P. Butts, J. Bowers, J.R.P. Webster, R.K. Heenan, J. Colloid Interface Sci. 307 (2007) 455.
[32] J.J. Wang, H.Y. Wang, S.L. Zhang, H.C. Zhang, Y. Zhao, J. Phys. Chem. B 111 (2007) 6181.
[33] M. Blesic, M.H. Marques, N.V. Plechkova, K.R. Seddon, L.P.N. Rebelo, A. Lopes, Green Chem. 9 (2007) 481.
[34] B. Dong, N. Li, L.Q. Zheng, L. Yu, T. Inoue, Langmuir 23 (2007) 4178.
[35] R. Vanyúr, L. Biczók, Z. Miskolczy, Colloids Surf., A 299 (2007) 256.
[36] A. Modaressi, H. Sifaoui, M. Mielcarz, U. Domańska, M. Rogalski, Colloids Surf., A 302 (2007) 181.
[37] T. Singh, A. Kumar, J. Phys. Chem. B 111 (2007) 7843.
[38] O.A. El Seoud, P.A.R. Pires, T. Abdel-Moghny, E.L. Bastos, J. Colloid Interface Sci. 313 (2007) 296.
[39] L. Gaillon, J. Sirieix-Plénet, P. Letellier, J. Sol. Chem. 33 (2004) 1333.
[40] J. Bowers, C.P. Butts, P.J. Martin, M.C. Vergara-Gutierrez, R.K. Heenan, Langmuir 20 (2004) 2191.
[41] J. Sirieix-Plénet, L. Gaillon, P. Letellier, Talanta 63 (2004) 979.
[42] Z. Miskolczy, K. Sebők-Nagy, L. Biczók, S. Göktürk, Chem. Phys. Lett. 400 (2004) 296.
[43] G. Law, P.R. Watson, Langmuir 17 (2001) 6138.
[44] K.O. Evans, Colloids Surf., A 274 (2006) 11.
[45] E. Ghasemian, M. Najafi, A.A. Rafati, Z. Felegari, J. Chem. Thermodyn. 42 (2010) 962.
[46] O. Myakonkaya, J. Eastoe, K.J. Mutch, S.E. Rogers, R.K. Heenan, I. Grillo, Langmuir 25 (2009) 2743.
[47] K. Trickett, D.Z. Xing, J. Eastoe, R. Enick, A. Mohamed, M.J. Hollamby, S. Cummings, S.E. Rogers, R.K. Heenan, Langmuir 26 (2010) 4732.
[48] A. Mohamed, K. Trickett, S.Y. Chin, S. Cummings, M. Sagisaka, L. Hudson, S. Nave, R. Dyer, S.E. Rogers, R.K. Heenan, J. Eastoe, Langmuir 26 (2010) 13861.
[49] P. Brown, C. Butts, R. Dyer, J. Eastoe, I. Grillo, F. Guittard, S.E. Rogers, R.K. Heenan, Langmuir 27 (2011) 4563.
[50] M. Sagisaka, S. Iwama, S. Hasegaw, A. Yoshizawa, A. Mohamed, S. Cummings, S.E. Rogers, R.K. Heenan, J. Eastoe, Langmuir 27 (2011) 5772.
[51] M.A. Firestone, J.A. Dzielawa, P. Zapol, L.A. Curtiss, S. Seifert, M.L. Dietz, Langmuir 18 (2002) 7258.
[52] T. Inoue, B. Dong, L.Q. Zheng, J. Colloid Interface Sci. 307 (2007) 578.
[53] W. Ostwalds, Z. Phys. Chem. 22 (1897) 286.
[54] E.B. Sirota, A.B. Herhold, Science 283 (1999) 529.
[55] L.B. Li, J. Groenewold, S.J. Picken, Chem. Mater. 17 (2005) 250.
[56] F.G. Wu, L. Chen, Z.W. Yu, J. Phys. Chem. B 113 (2009) 869.
[57] F.G. Wu, N.N. Wang, Z.W. Yu, Langmuir 25 (2009) 13394.
[58] S. Sasaki, J. Phys. Chem. B 111 (2007) 2473.
[59] V.K. Aswal, P.S. Goyal, Chem. Phys. Lett. 368 (2003) 59.
[60] F.G. Wu, J.S. Yu, S.F. Sun, Z.W. Yu, Langmuir 27 (2011) 14740.
[61] F.G. Wu, Q. Jia, R.G. Wu, Z.W. Yu, J. Phys. Chem. B 115 (2011) 8559.
[62] R. Klein, G.J.T. Tiddy, E. Maurer, D. Touraud, J. Esquena, O. Tache, W. Kunz, Soft Matter 7 (2011) 6973.
[63] Z.W. Yu, W.P. Williams, P.J. Quinn, Arch. Biochem. Biophys. 332 (1996) 187.
[64] Z.W. Yu, P.J. Quinn, Biophys. J. 69 (1995) 1456.
[65] M.W. Zhao, Y.A. Gao, L.Q. Zheng, J. Phys. Chem. B 114 (2010) 11382.
[66] L.Y. Wang, X. Chen, Y.C. Chai, J.C. Hao, Z.M. Sui, W.C. Zhuang, Z.W. Sun, Chem. Commun. (2004) 2840.
[67] Z.N. Wang, F. Liu, Y.A. Gao, W.C. Zhuang, L.M. Xu, B.X. Han, G.Z. Li, G.Y. Zhang, Langmuir 21 (2005) 4931.
[68] A. Klaus, G.J.T. Tiddy, D. Touraud, A. Schramm, G. Stühler, W. Kunz, Langmuir 26 (2010) 16871.
[69] R.N.A.H. Lewis, R.N. McElhaney, in: A.M. Dopico (Ed.), Methods in Molecular Biology, vol. 400, Humana Press, Totowa, NJ, 2007, p. 207.
[70] F.G. Wu, Z.W. Yu, G. Ji, Langmuir 27 (2011) 2349.
[71] F.G. Wu, J.J. Luo, Z.W. Yu, Langmuir 26 (2010) 12777.
[72] F.G. Wu, N.N. Wang, J.S. Yu, J.J. Luo, Z.W. Yu, J. Phys. Chem. B 114 (2010) 2158.

[73] F.G. Wu, N.N. Wang, L.F. Tao, Z.W. Yu, J. Phys. Chem. B 114 (2010) 12685.
[74] A. Wulf, K. Fumino, R. Ludwig, J. Phys. Chem. A 114 (2010) 685.
[75] Q.G. Zhang, N.N. Wang, Z.W. Yu, J. Phys. Chem. B 114 (2010) 4747.
[76] N.N. Wang, Q.G. Zhang, F.G. Wu, Q.Z. Li, Z.W. Yu, J. Phys. Chem. B 114 (2010) 8689.
[77] K. Fumino, A. Wulf, R. Ludwig, Phys. Chem. Chem. Phys. 11 (2009) 8790.
[78] L.Q. Zhang, Z. Xu, Y. Wang, H.R. Li, J. Phys. Chem. B 112 (2008) 6411.
[79] K. Fumino, A. Wulf, R. Ludwig, Angew. Chem., Int. Ed. 47 (2008) 3830.
[80] K. Fumino, A. Wulf, R. Ludwig, Angew. Chem., Int. Ed. 47 (2008) 8731.
[81] A. Yokoczki, D.J. Kasprzak, M.B. Shiflett, Phys. Chem. Chem. Phys. 9 (2007) 5018.
[82] K. Fumino, A. Wulf, R. Ludwig, ChemPhysChem 8 (2007) 2265.
[83] J. Kiefer, J. Fries, A. Leipertz, Appl. Spectrosc. 61 (2007) 1306.
[84] T. Köddermann, C. Wertz, A. Heintz, R. Ludwig, Angew. Chem., Int. Ed. 45 (2006) 3697.
[85] T. Köddermann, C. Wertz, A. Heintz, R. Ludwig, ChemPhysChem 7 (2006) 1944.
[86] J.D. Tubbs, M.M. Hoffmann, J. Solution Chem. 33 (2004) 381.
[87] J.N. Israelachvili, D.J. Mitchell, B.W. Ninham, Faraday Trans. II 72 (1976) 1525.
[88] C. Tanford, J. Phys. Chem. 76 (1972) 3020.
[89] S. Sasaki, J. Phys. Chem. B 113 (2009) 8545.
[90] S. Sasaki, J. Phys. Chem. B 114 (2010) 11039.